Integer and fractional quantum hall effects in lattice magnets

Venderbos, J.W.F.

CHAPTER 7

TRIANGULAR LATTICE FRACTIONAL CHERN INSULATOR MODEL

7.1 Introduction

The Fractional Quantum Hall effect is one of the most peculiar and intriguing states of matter. Discovered in 1982 [10], not very long after the Integer Quantum Hall effect [75], it has continued to fascinate condensed matter physicists until the present day. The key experimental characteristic of the integer quantum Hall effect is the emergence of quantum Hall plateaus, plateaus in the off diagonal Hall conductivity σ_{xy} as function of magnetic field at integer multiples of the quantum of conductance e^2/h, while the longitudinal conductivity vanishes. At particularly strong magetic fields, plateau structures are observed at non-integer, i.e. fractional (for the purpose of this chapter we will assume rational, p/q) values and these are known as the Fractional Quantum Hall effect. While the integer effect can be understood purely in terms of single-particle state physics (see also Chapter 1), its fractional counterpart is a consequence of electron-electron interaction. Even more, as the degeneracy of a magnetic Landau level scales with the magnetic field, in a very strong magnetic field all electrons will be in the lowest Landau level (LLL) and the repulsive Coulomb interaction will be the only remaining energy scale. Hence, even though superficially similar judging from their experimental signature, the integer and fractional

Quantum Hall effect are fundamentally distinct, with the fractional QHE presenting a much more difficult problem due to its quartic Hamiltonian structure.

The fascination with the Fractional Quantum Hall effect derives from its special features as a rather exotic quantum state of matter. The fractional Quantum Hall state constitutes an incompressible liquid, which sets it apart from states of matter that are classified according to broken symmetries represented by a local order parameter. An example of the latter, which naturally competes with the fractional Quantum Hall state in the presence of strong electron repulsion, is the Wigner crystal, a charge ordered state. The fractional Quantum Hall ground state is topologically ordered, implying a ground state degeneracy which depends on the topology of the manifold on wich it lives (torus, sphere, ect.). The FQH effective field theory is therefore not of Ginzburg-Landau type, but is instead a topological Chern-Simons field theory accounting phenomenologically for its physical characterics. In addition, the quasiparticles of these states have fractional charge and obey anyonic statistics, [138, 139] which can be either Abelian or non-Abelian, the latter fulfilling an essential condition for fault-tolerant quantum computation. [129]. In particular these quasiparticle properties have attracted a great deal of attention and have triggered considerbable effort in uncovering the deep physics of the FQHE.

As a consequence of the recent and tremendous surge in interest in topological states of matter, caused by the discovery of topological insulators [12,111], new directions in fractional quantum Hall physics have been explored. In particular, since the topological insulators can be regarded as generalizations of the quantum anomalous Hall insulator, which belongs to the IQH universality class, the following question presented itself: can the FQHE be generalized to situations where external magnetic fields are absent and lattice effects cannot be ignored? This question was first addressed by [87,108,113]. In case of the continuum FQHE, Hilbert space is organized according to the Landau level spectrum which originates from the magnetic field. Adding interactions to the LLL yields the FQHE. In case of a lattice model described by a tight-binding hamiltonian $\hat{H}$ the first prerequisite for any hope of a possible generalized FQHE is the presence of isolated bands with nontrivial topology. Or, in other words, the band structure corresponding to $\hat{H}$ needs consist of a band with nonzero Chern number C (see Chapter 1), separated from other bands by a full energy gap. That such Hamiltonians exist in principle has been demonstrated already long ago by Haldane in 1988 [76], but the past decade has witnessed an impressive effort in devising proposals for realizing such a Hamiltonian in experimentally accessible conditions. One such realization may be found in strongly spin-orbit coupled semiconductor materials that are ferromagnetically ordered [77, 82]. Another possibility arises through the coupling of itinerant electrons to localized magnetic moments [85], for example the Kondo-lattice model on the triangular lattice supports a non-trivial magnetic texture, which induces an integer-quantized Hall conductivity of the itin-

erant electrons [30]. Note that nonzero Chern number C immediately implies the breaking of time-reversal symmetry, which is reassuring, as the uniform magnetic field breaks time-reversal in the continuum.

While the above is unambiguously sufficient to generalize integer quantum Hall physics to lattice systems without fields, fractional quantum Hall physics puts more restrictions on potential generalization schemes. If we focus on a band that has nonzero Chern number (is has become custom to call such a band *Chern band*), and compare it more closely to a Landau level, we observe that the Chern band is generally dispersive, a Landau level however is perfectly flat, i.e. all single-particle states have the same energy. This is of considerable significance, as it renders the interactions to be the only energy scale of the problem en thus by definition the dominant one. The interactions select the fractional quantum Hall liquid out of the macroscopically degenerate manifold of single-particle states. Adding interactions to a Chern band would seem to lead to a competition between kinetic and interaction energy scales, which potentially spoils the emergence of a liquid state. Hence, in order for the Chern band to mimick the Landau level as much as possible, one should require the former to have a very small bandwidth W as compared to the interaction strength V. To put it differently, minimally dispersive or *flat* Chern bands are expected to be the best candidates for hosting a lattice FQHE. Furthermore, the ordinary FQHE is most clearly observed in a strong magnetic field, which causes a large energy gap between Landau levels and concentrates all electrons in the LLL. Landau level mixing is negligible. It would consequently seem natural to demand that that band gap Δ which separates the Chern band from any other band is much larger than the interaction energy scale V. Summarizing, the following hierarchy of energy scales would need to be fulfilled to provide proper conditions for fractional quantum Hall physics confined to a Chern band

$$\Delta \gg V \gg W, \quad F \equiv \Delta/W \gg 1. \tag{7.1}$$

With this perspective in mind, the first studies of FQH generalization were undertaken [87, 104, 105, 108, 113, 131, 140]. Chern insulator models with the correct energy scale hierarchy were identified and first signatures of fractional quantum Hall type physics were obtained with numerical methods. Starting from a Chern insulator given by the non-interacting Hamiltonian

$$\hat{H}_{\text{CI}} = \sum_{\vec{K}} \hat{\psi}^{\dagger}_{\alpha}(\vec{k}) \mathcal{H}^{\alpha\beta}(\vec{k}) \hat{\psi}_{\beta}(\vec{k}), \tag{7.2}$$

interactions were added by including

$$\hat{H}_{\text{int}} = \sum_{ij} V^{\alpha\beta}_{ij} \hat{n}_{i\alpha} \hat{n}_{j\alpha} = \sum_{\vec{q}} V^{\alpha\beta}(\vec{q}) \hat{\rho}_{\alpha}(\vec{q}) \hat{\rho}_{\beta}(-\vec{q}), \tag{7.3}$$

and the standard approach has been to isolate the Chern band explicitly and project the interactions into that band. This requires normal ordering first and then projecting onto band n with corresponding energy $E_n(\vec{k})$, obtained afterdiagonalization of the Bloch Hamiltonian $\mathcal{H}(\vec{k})$. The eigenstates are $|\vec{k}, n\rangle = \hat{\gamma}_n^\dagger(\vec{k})|0\rangle$. The normal mode operators and orbital operators are related by a matrix $U(\vec{k})$ that contains the eigenvectors of the matrix $\mathcal{H}(\vec{k})$ in its columns, $\hat{\gamma}_n^\dagger(\vec{k}) = \hat{\psi}_\alpha^\dagger(\vec{k})U_{\alpha n}(\vec{k})$ with $\mathcal{H}_{\alpha\beta}(\vec{k})U_{\beta n}(\vec{k}) = E_n(\vec{k})U_{\alpha n}(\vec{k})$. The interaction becomes

$$\hat{H}_{\text{int}} = \frac{1}{N}\sum_{\vec{k},\vec{k}'}\sum_{\vec{q}} V^{\alpha\beta}(\vec{q})\hat{\psi}_\alpha^\dagger(\vec{k}+\vec{q})\hat{\psi}_\beta^\dagger(\vec{k}'-\vec{q})\hat{\psi}_\beta(\vec{k}')\hat{\psi}_\alpha(\vec{k})$$

$$= \frac{1}{N}\sum_{\vec{k},\vec{k}'}\sum_{\vec{q}} V^{n_1n_2n_3n_4}(\vec{q},\vec{k},\vec{k}')\hat{\gamma}_{n_1}^\dagger(\vec{k}+\vec{q})\hat{\gamma}_{n_2}^\dagger(\vec{k}'-\vec{q})\hat{\gamma}_{n_3}(\vec{k}')\hat{\gamma}_{n_4}(\vec{k}) \qquad (7.4)$$

with

$$V^{n_1n_2n_3n_4}(\vec{q},\vec{k},\vec{k}') =$$
$$\sum_{\alpha,\beta} V^{\alpha\beta}(\vec{q})U_{n_1\alpha}^\dagger(\vec{k}+\vec{q})U_{n_2\beta}^\dagger(\vec{k}'-\vec{q})U_{\beta n_3}(\vec{k}')U_{\alpha n_4}(\vec{k}). \qquad (7.5)$$

From the general form of this expression it is clear that the interaction contains interband scattering events. With the separation of energy scales properly in place it has become common practice to focus exclusively on the given Chern band n, neglecting the its dispersion, i.e. $E_n(\vec{k}) \to \overline{E}_n$ and keeping only the terms $n_1 = n_2 = n_3 = n_4 = n$. This approach, which then lends itself to exact diagonalization (ED) studies is in contrast to the method explained later in this chapter and implemented in [107, 141]. In the final section of this chapter we discuss the numerical signatures of FQH physics in these Chern insulators in somewhat more detail.

In the wake of these first steps towards a lattice generalization of the FQHE – quickly dubbed the *Fractional Chern Insulator* (FCI) – the question of what constitutes good Chern bands has been addressed in more detail. Is it just the hierarchy of energy scales in a Chern insulator, or can and should one identify constraints of an entirely different quality? This specific question was first considered by [142] and soon after reconsidered by [143–145]. The central results of these works is the derivation of constraint on Berry curvature fluctuations of the Chern insulator model. The key idea is that in the continuum the density operators projected onto the LLL satisfy the GMP algebra (see again Chapter 1) and in order to keep the analogy with the LLL upright, the density operators of a Chern insulator projected into the (nearly flat) Chern band, should obey an equivalent algebraic relation. The orbital dependent

density operator is given by

$$\hat{\rho}_\alpha(\vec{q}) = \frac{1}{\sqrt{N}} \sum_{\vec{k}} \hat{\psi}^\dagger_\alpha(\vec{k}+\vec{q})\hat{\psi}_\alpha(\vec{k}), \tag{7.6}$$

and projecting this into the Chern band labeled by n, summing over α, gives

$$\tilde{\rho}(\vec{q}) \equiv \hat{P}_n\hat{\rho}(\vec{q})\hat{P}_n = \frac{1}{\sqrt{N}} \sum_{\vec{k},\alpha} U^\dagger_{n\alpha}(\vec{k}+\vec{q})U_{\alpha n}(\vec{k})\hat{\gamma}^\dagger_n(\vec{k}+\vec{q})\hat{\gamma}_n(\vec{k}) \tag{7.7}$$

The central result obtained from aforementioned investigation of the algebraic relations of projected density operators is that in the long wave-length limit, i.e. $\vec{q}, \vec{w}$ small, and in cases when the Berry curvature may be approximated by its average, the $\tilde{\rho}(\vec{q})$ satisfy

$$[\tilde{\rho}(\vec{q}), \tilde{\rho}(\vec{w})] \approx -i(\vec{q}\times\vec{w})\cdot\hat{z}\frac{2\pi C}{(2\pi/a)^2}\tilde{\rho}(\vec{q}+\vec{w}). \tag{7.8}$$

This is identical to the long wave-length limit of the GMP algebra obeyed by projected density operators in the LLL. The crucial insight that the algebra of density operators reveals, is that once the GMP is valid in the Chern band for long wavelengths, one may assume it to be valid at all wave-lengths in the thermodynamic limit, thereby establishing an a posteriori correspondence between the FCI and the FQH physics [142, 143].

Having discussed in considerable detail the prerequisites for FCI physics in Chern insulators, we state the purpose and content of this chapter. Previous chapters have demonstrated how nearly flat topological bands can arise in multi-orbital models of correlated oxides. In this chapter we map the multi-orbital model onto an effective single-orbital model, which nevertheless captures the essential features of the Chern insulator and subsequently can be used for detailed numerical study into possible FCI signatures. It will be argued that obtained triangular lattice Chern insulator shows robust features of FCI physics.

7.2 Multi-orbital nearly flat band model

In previous chapters it was shown that both e_g and t_{2g} orbital manifolds in octahedral coordination can reduce the bandwidth of topologically nontrivial bands. For a schematic illustration of orbital degeneracy in d-electron systems see Fig. 6.2. In particular, this was discussed for the spin-chiral phase arising in Kondo-lattice models on the triangular lattice at quarter and three-quarter fillings. While the flat band of

interest mixes both the $3z^2 - r^2$ and the $x^2 - y^2$ orbitals in the e_g case, it is dominated by a particular orbital state in the t_{2g} manifold, the a_{1g} state. We recall that the trigonal crystal field splits the t_{2g} manifold in an e_g'-doublet and the nondegenerate a_{1g} level. The fact that the flat mean-field Chern band of the multi-orbital model has predominantly a_{1g} character suggests that one may capture the essential physics. The program of this chapter is to systematically arrive at a simple Chern insulator model that may be used for extensive numerical calculations probing its suitability as host of FCI states. We will start from realistic multi-orbital models, in particular the band structure obtained from the mean-field treatment of local Coulomb interaction terms, as detailed in the previous chapter.

We focus exclusively on the t_{2g} triangular lattice model. In addition to an orbital degree of freedom, we consider coupling to a localized spin $\vec{S}_i$, modelled by a Kondo-lattice model, where the kinetic energy is given by hopping elements $t_{ij}^{\alpha\beta}$ taken from the matrices Eq. (6.1) or Eq. (6.4). This situation is described by

$$\hat{H} = \sum_{\langle i,j\rangle,\sigma} t_{ij}^{\alpha\beta} \hat{\psi}_{i\sigma\alpha}^{\dagger} \hat{\psi}_{j\sigma\beta} - J_{\text{Kondo}} \sum_{i,\alpha} \vec{S}_i \cdot \vec{\hat{s}}_{i\alpha} \tag{7.9}$$

where α and β are orbital indices, $\hat{\psi}_{i\sigma\alpha}$ ($\hat{\psi}_{i\sigma\alpha}^{\dagger}$) annihilates (creates) an electron with spin σ in orbital α at site i, and $\vec{\hat{s}}_{i\alpha}$ is the corresponding vector of orbital electronic spin operators. J_{Kondo} couples the itinerant electrons to a generic localized spin $\vec{S}_i$, the origin of which is left unspecified for the moment, but will be discussed extensively later. (It will turn out to be the spin degree of freedom of the t_{2g} electrons themselves, as may be expected from 6). The coupling is assumed to be FM, as one would expect from Hund's-rule coupling. However, we are furthermore going to consider $\vec{S}_i$ as a *classical* spin, in which case AFM coupling to $\vec{S}_i$ would lead to the equivalent results.

7.2.1 Integrating out the spin-degree of freedom

For classical spins and large J_{Kondo}, it is convenient to go over to a *local* spin-quantization axis, where "↑" ("↓") refers to parallel (antiparallel) orientation of the electron's spin to the local axis. This simplifies the Kondo term to

$$\hat{H}_{\text{Kondo}} = -J_{\text{Kondo}} \sum_{i,\alpha} \vec{S}_i \cdot \vec{\hat{s}}_{i,\alpha} = -\frac{J_{\text{Kondo}}}{2} \sum_{i,\alpha} (\hat{n}_{\alpha\uparrow} - \hat{n}_{\alpha\downarrow}) \ , \tag{7.10}$$

where $\hat{n}_{\alpha}^{\uparrow}$ ($\hat{n}_{\alpha}^{\downarrow}$) is the electron density at site i in orbital α with spin (anti-) parallel to the localized spin. This local spin definition is particularly convenient when going to the limit of large J_{Kondo}, where one immediately finds the low-energy states as given by only "↑" electrons.

On the other hand, the fact that the spin-quantization axis is not the same at all sites implies that the hopping no longer conserves the new spin. Instead, hopping acquires as spin-dependent factor $t_{ij}^{\alpha\beta} \to t_{ij}^{\alpha\beta\sigma\sigma'} = t_{ij}^{\alpha\beta} u_{ij}^{\sigma\sigma'}$, [28] with

$$u_{ij}^{\uparrow\uparrow} = c_i c_j + s_i s_j e^{-i(\phi_i - \phi_j)}, \tag{7.11}$$

$$u_{ij}^{\downarrow\downarrow} = c_i c_j + s_i s_j e^{i(\phi_i - \phi_j)}, \tag{7.12}$$

$$u_{ij}^{\sigma\bar{\sigma}} = \sigma(c_i s_j e^{-i\sigma\phi_j} - c_j s_i e^{-i\sigma\phi_i}),$$

where $\bar{\sigma} = -\sigma$ and $c_i = \cos\theta_i/2$, $s_i = \sin\theta_i/2$ and the set of angles $\{\theta_i\}$ and $\{\phi_i\}$ are the polar and azimuthal angles corresponding to $\{\vec{S}_i\}$, respectively. As one can see, these effective hoppings can become complex, and it has been shown that non-coplanar spin configurations can endow the electronic bands with a nontrivial topology [30, 85].

In line with the approach extensive outlined elsewhere in this thesis, we may assume strong coupling between the local moments and the itinerant electrons and take the limit of infinite Hund's rule coupling. In this case, one only keeps the $\uparrow$ electrons parallel to the local spin-quantization axis and electrons effectively become spinless fermions. For the chiral spin pattern in Fig. 6.4, which has been found as the ground state of triangular Kondo-lattice models [30–32, 100], the Berry phases between the four sites of the magnetic unit cell can be parametrized as

$$u_{1,2}^{\uparrow\uparrow} = u_{3,4}^{\uparrow\uparrow} = \frac{1}{\sqrt{3}}, \quad u_{1,3}^{\uparrow\uparrow} = -u_{2,4}^{\uparrow\uparrow} = \frac{1}{\sqrt{3}} \tag{7.13}$$

$$u_{2,3}^{\uparrow\uparrow} = u_{4,1}^{\uparrow\uparrow} = -u_{3,2}^{\uparrow\uparrow} = -u_{1,4}^{\uparrow\uparrow} = \frac{i}{\sqrt{3}}.$$

Constructing the tight-binding hopping Hamiltonian from these effective hoppings of the now effectively spinless fermions (which still have an orbital degree of freedom) reveals that even though the unit cell corresponding to the spin configuration contains four sites, the unit cell of the fermions can be reduced to two sites.

Combining the phases Eq. (7.13) with the hoppings given by Eqs. (6.1) or (6.4) and the crystal-field splitting Eq. (6.2) still gives a non-interacting model that can be easily solved in momentum space. One finds that large $|\Delta_{\mathrm{JT}}|$, see Eq. (6.2), strongly reduces the dispersion of one subband. This can also be seen in Fig. 7.1(a), which shows the one-particle energies obtained on a cylinder. Figure 7.1(a) also reveals the edge states crossing some gaps, indicating the topologically nontrivial nature of these bands. Calculating Chern numbers C corroborates this and gives $C = \pm 1$. The band flatness can be expressed in terms of a figure of merit

$$F = \frac{\min(\overline{\Delta}_{\mathrm{JT}}, \Delta_c)}{W}, \tag{7.14}$$

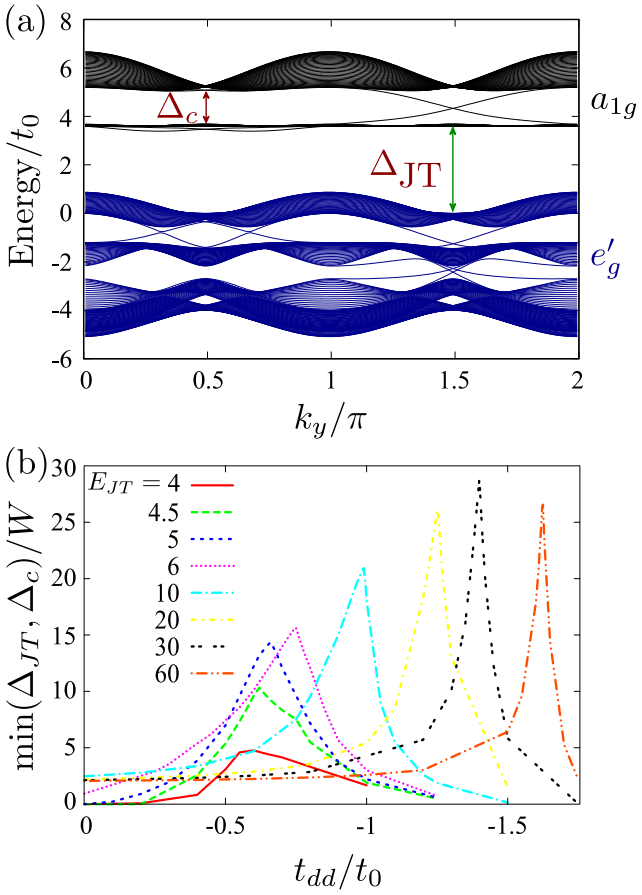

Figure 7.1: Flat lower chiral subband in the Kondo-lattice model with infinite Hund's rule coupling (double-exchange model). (a) Shows the one-particle energies of three t_{2g} orbitals coupled to localized spins, where the latter form a spin-chiral phase on a triangular lattice, [30–32, 100] see Fig. 6.4. The system is a cylinder, i.e., periodic boundary conditions along y-direction and open boundaries along x. The horizontal axis is the momentum in the direction with periodic boundaries. The gaps $\Delta_{\rm JT}$ and Δ_c denote the gaps due to crystal-field splitting $E_{\rm JT}$ and to the chiral spin state. (b) shows the figure of merit M, see Eq. (7.14), for the lower a_{1g} subband. The curves for crystal-field splittings $E_{\rm JT} = 4, 4.5$, and 5 were already given in Fig. 3(b) of Ref. [**?**] and are repeated here for convenience.

where $\overline{\Delta}_{\mathrm{JT}}$ and Δ_c are the two gaps separating the narrow band of interest from the other orbitals and from the subband with opposite Chern number and W is the width of the narrow band. As was pointed out in chapter 5, the lower subband can here become very flat, and as can be seen in Fig. 7.1(b), the flatness can be further improved by going to larger crystal fields and reaches values $M \approx 28$.

7.2.2 Integrating out the orbital degree of freedom

As these very flat bands can be achieved for large separation E_{JT} between the a_{1g} and e_g' states and as the band of interest then has almost purely a_{1g} character, it is natural to assume that one should be able to capture the most relevant processes with an effective a_{1g} model. (This is in contrast to the situation starting from e_g orbitals, where one finds intermediate E_{JT} to be optimal. In that case, the nearly flat bands can only be obtained if *both* orbitals contribute weight and one cannot easily reduce the situation to a one-band system.)

The impact of the e_g' levels on the effective a_{1g} dispersion can be taken into account in second-order perturbation theory. This includes processes where a hole hops from the a_{1g} orbital at site i to an e_g' state at j and back again to an a_{1g} state at a third site i', which may or may not be the same as i. The denominator of these terms is the crystal-filed energy E_{JT} and the numerator is obtained from the products $\widetilde{T}_i^{ab}\widetilde{T}_j^{ba} + \widetilde{T}_i^{ac}\widetilde{T}_j^{ca}$ (with a designating a_{1g} and b, c the e_g' states). In order to evaluate the second-order hopping between sites i and i', these orbital hoppings have to be multiplied by the product of the Berry phases $u_{i,j}^{\uparrow\uparrow}$ and $u_{j,i'}^{\uparrow\uparrow}$ from Eq. (7.13) for all paths connecting i and i' via one intermediate site $j \neq i, i'$. Due to destructive interference, processes connecting NN and next-nearest neighbor (NNN) sites cancel while effective third-neighbor hopping, where there is only one path, remains. Since third-neighbor spins in the chiral phase are always parallel, the total Berry phase of this process is 1 in all directions, however, the hopping via a spin of different orientation in the middle reduces the hopping amplitude by $|u^{\uparrow\uparrow}|^2 = 1/3$, leading to

$$t_3 = -\frac{2(t_0 - t_{dd})^2}{27\Delta_{\mathrm{JT}}} \,. \tag{7.15}$$

A third-neighbor hopping $\propto \sum_i \cos 2\vec{k} \cdot \vec{a}_i$ turns out to have almost the same dispersion as the chiral subbands and can consequently almost cancel it in one subband. As its strength can be tuned by t_{dd} and Δ_{JT}, very flat subbands can be achieved, see Fig. 7.1(b).

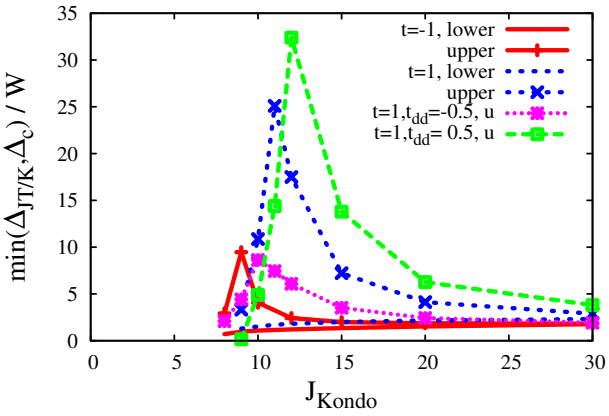

Figure 7.2: Figure of merit M, see Eq. (7.14), for finite Hund's-rule coupling J_{Kondo}/t_0 and $E_{\text{JT}} = 6t_o$. The bands designated as "upper" and "lower" refer to the two subbands of the a_{1g} states with spin parallel to the localized spin, which are separated by the gap opening in the spin-chiral phase, see Fig. 7.1(a).

7.2.3 Mapping the mean-field solution to a Chern insulator

While the previous section has illustrated how one can understand the occurrence of nearly flat bands in a three-orbital double-exchange model, i.e., for infinite Hund's rule coupling to some localized spins, this section will discuss finite Hund's rule and take the single-particle spectrum obtained from the mean-field calculation as a starting point for deriving an effective hopping model. Figure 7.2 shows the figure of merit for the band flatness Eq. (7.14) for a few sets of hopping parameters and for $\Delta_{\text{JT}} = 6t_0$ depending on Hund's rule coupling J_{Kondo} to the localized spin, see Eq. (7.10). As can be seen in Fig. 7.2, the *upper* subband of the a_{1g} sector can now become nearly flat. (For $J_{\text{Kondo}} \gg |\Delta_{\text{JT}}|$, one can of course still find flat lower subbands, as discussed above.)

The flatness of the upper subband can be explained by similar effective longer-range hoppings in second-order perturbation theory, this time also taking into account intermediate states with an electron in the upper Kondo band, i.e. with antiparallel spin. These additional terms can go either via the a_{1g} or via the e'_g orbitals and involve combined Berry phases of the form $u_{ij}^{\uparrow\downarrow} u_{ji'}^{\downarrow\uparrow}$. Again, one has to sum over all possible

intermediate sites j and finds

$$t_1 = \frac{3t+\delta t}{3} + 2\frac{(3t+\delta t)^2}{9}\frac{1}{E_2} - 2\frac{\delta t^2}{9}\frac{1}{E_3}, \tag{7.16}$$

$$t_2 = 2\frac{(3t+\delta t)^2}{9}\frac{1}{E_2} - 2\frac{\delta t^2}{9}\frac{1}{E_3}, \tag{7.17}$$

$$t_3 = 2\frac{(3t+\delta t)^2}{27}\frac{1}{E_2} + 4\frac{\delta t^2}{27}\frac{1}{E_3} + 2\frac{\delta t^2}{27}\frac{1}{E_1}\ . \tag{7.18}$$

The NN, NNN and third-neighbor hoppings are here denoted by t_1, t_2, and t_3. $E_1 = \Delta_{\text{JT}}$, $E_2 = J_{\text{Kondo}}$, and $E_3 = J_{\text{Kondo}} - \Delta_{\text{JT}}$ give the excitation energies of the intermediate states with (i) a hole in the e_g' states with spin parallel, (ii) an electron in the a_{1g} states with spin anti-parallel and (iii) an electron in an e_g' state with spin anti-parallel. Like the bare NN hopping, these effective hopping-matrix elements acquire an additional Berry phase $u_{ii'}^{\uparrow\uparrow}$ in the Hamiltonian, which only depends on the relative orientation of spins on the initial and final sites. NNN hopping t_2 via the upper Kondo band does not drop out, and NN hopping becomes renormalized.

The flat chiral subbands that have been observed in a three-orbital t_{2g} Hubbard model on the triangular lattice [107] arise in situations similar to the finite-J_{Kondo} scenario. Above we have shown that a mapping to the Kondo-lattice model can be constructed and that the physics of the flat band is captured by taking the other into account perturbatively. The key point of the mapping is the observation that large crystal-field splitting Δ_{JT}, see (6.2), leads to an orbital-selective Mott-insulator, where the e_g' levels are half-filled and far from the Fermi level, while the states near the Fermi level have almost only a_{1g} character. The orbital degree of freedom is consequently quenched, because orbital occupations are already fully determined. A charge degree of freedom remains, as the a_{1g} orbital contains one electron per two sites. Charge fluctuations of the half-filled e_g levels, however, are suppressed due to the large Mott gap between their occupied and empty states. They can thus be described as a spin degrees of freedom, and the situation is further simplified, because they form a total spin with $S = 1$ due to Hund's rule. The a_{1g} electron is likewise coupled via FM Hund's rule to this spin. This situation – mobile carriers coupled via FM Hund's rule to localized spin degrees of freedom – is well described by a FM Kondo-lattice model.

7.3 Triangular lattice Chern Insulator

As we have discussed in the previous section, the most realistic route to nearly flat bands with nontrivial topology on the triangular lattice arises at finite Hubbard/Kondo

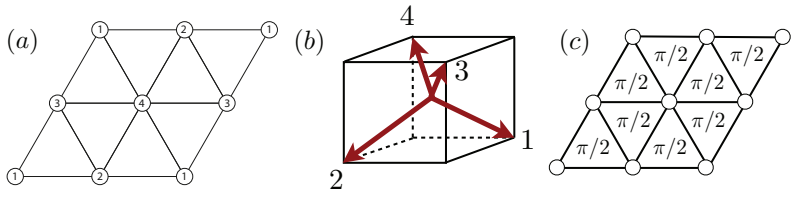

Figure 7.3: (a) Schematic illustration of the 4-site unit cell of the magnetic configuration on the triangular lattice where the the number labels correspond to the spins represented in (b). (c) shows the effective single-orbital spinless model, which is that of fermions hopping on the triangular lattice with each triangle threaded by a flux of $\phi = \pi/2$

coupling, where effective second-neighbor hopping is generated in addition to NN and third-neighbor terms. However, the exposition in previous sections has demonstrated that all essential features of the band structure can be captured by using just NN and third-neighbor hoppings. As the purpose of this chapter was to arrive a simple Chern insulator model that both captures the essential features of a more realistic multi-orbital model of correlated oxides, and meets all requirements for showing FCI physics, we adopt the a_{1g} model with NN and third-NN hopping for simplicity.

The essential ingredients for the triangular lattice Chern insulator model are spinless fermions coupled to an effective compact $U(1)$ gauge field A_{ij}. In other words, the fermions hop in the presence of an effective flux threading the triangles. The Hamiltonian of these fermions in momentum space is given by

$$\mathcal{H}_{\rm CI}(\vec{k}) = 2t \sum_j \cos k_j \, \tau^j + 2t' \sum \tau^0 \cos 2k_j \ , \tag{7.19}$$

where $\vec{a}_j$ ($j = 1, 2, 3$) denote the unit vectors on the triangular lattice, $k_j \equiv \vec{k} \cdot \vec{a}_j$, and t and t' are the NN and third-neighbor hopping, which can be related to Eqs. (7.13) and (7.15) for the double-exchange scenario, to Eqs. (7.16) and (7.18) for finite onsite interactions, or which can be taken as fit parameters. Pauli matrices σ^j and unit matrix σ^0 refer to the two sites of the electronic unit cell in the chiral state. The unit cell and the topologically non-trivial bands are due to the symmetry breaking involved in the underlying magnetic order. The dispersion of Eq. (7.19) is

$$E_\pm(\vec{k}) = \pm 2t \sqrt{\sum_j \cos^2 k_j} + 2t' \sum_j \cos 2k_j . \tag{7.20}$$

Figure 7.3 shows pictorially how the lattice fermion model with fluxes is connected

to the spin ordered state. As panel (c) indicates, the Berry phases coming from the noncoplanar spins lead to a uniform flux arrangement that is equivalent to a uniform magnetic field perpendicular to the lattice. This is in contrast to other Chern insulator models which have a net flux of zero through the unit cell, while non-trivial fluxes do thread the individual plaquettes. This distinction must be qualified with a note of caution, however. On a lattice, the concept of "average" field is ill-defined, as one may always thread elementary flux quanta through selected plaquettes, which cannot change the physics, but does change the notion of net average field. In particular, in the present case we may group the triangles in sets of four and thread a additional flux of 2π through one of those four triangles, changing the plaquette flux to $-3\pi/2$ and making the average field zero. With this remark in mind, we choose however to think about this triangular Chern insulator model as fermions in a uniform magnetic field. From this connection we may immediately deduce that the unit cell should contain two atoms. The triangular lattice can be thought of as a square lattice with additional diagonal hoppings. It is a well established fact for the square lattice that in a magnetic field corresponding to flux $\phi = 2\pi\tilde{\phi}$, with $\tilde{\phi} = p/q$, the unit cell is q times larger. In this case a square plaquatte (two triangles) has flux $\tilde{\phi} = 1/4 + 1/4 = 1/2$ and the unit cell is doubled.

The Hamiltonian written in equation (7.19) is not in Bloch form, i.e. it does not satisfy $\mathcal{H}(\vec{k} + \vec{G}) = \mathcal{H}(\vec{k})$, where $\vec{G}$ is any reciprocal lattice vector. We wish to bring our Hamiltonian to Bloch form in order to probe to what extent we may expect this particular Chern insulator model to be a good candidate to host Fractional Chern insulator states. The introductory section already provided ways to interrogate the non-interacting Chern insulator model and will expand on that now. For convenience we make use of the aforementioned equivalence between the present Chern insulator model and lattice fermions on the square lattice in a magnetic field. The momentum space Hamiltonian of such fermions can be written as

$$\mathcal{H}(\vec{k}) = -t \begin{bmatrix} 2\cos k_y & -i(T_y T_x + T_y^*) - (1 + T_x) \\ i(T_y^* T_x^* + T_y) - (1 + T_x^*) & -2\cos k_y \end{bmatrix}, \quad (7.21)$$

with the definitions $T_x = e^{i2k_x}$ and $T_y = e^{ik_y}$. For details we refer the reader to Appendix B, and to references [146, 147]. As a consequence of the flux the reciprocal lattice vectors of the magnetic Brillouin zone are $\vec{G}_1 = (\pi, 0)$ and $\vec{G}_2 = (0, 2\pi)$ in units of the inverse lattice constant. By construction, see the Appendix B, this Hamiltonian is in Bloch form.

In the introduction it was shown that fluctuations in the Berry curvature of the band one wishes to address are expected to be critical for the potential emergence and stability of FCI states resembles ordinary Fractional Quantum Hall states. We therefore calculate the Berry curvature of the occupied band of model expressed in 7.21.

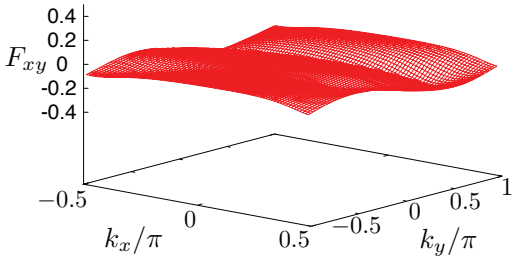

Figure 7.4: Plot of the Berry curvature in the rectified rectangular Brillouin zone of the triangular lattice Chern insulator model given by Hamiltonian (7.21).

For a tight-binding approach such as in the present case, the most convenient way to calculate the Berry curvature is borrowed from lattice gauge theory and was first introduced in [148]. The great advantage is the manifest invariance under electron wave function gauge transformations. This circumvents the cumbersome procedure of dividing the Brillouin zone in patches and finding a smooth gauge on each patch. If we take the lattice dimension in the i direction to be N_y, then we define a Brillouin zone grid of $N_x \times N_y$. We let $\vec{n} \in \mathbb{Z}_{N_x} \times \mathbb{Z}_{N_y}$ represent a site on the grid corresponding to momnetum $\vec{k} = (\pi n_x/N_x, 2\pi n_y/N_y)$. Then we define the so-called $U(1)$ *link* variables as

$$\mathcal{A}_i(\vec{n}) = \frac{\langle n, k_{\vec{n}} | n, k_{\vec{n}+\vec{u}_i} \rangle}{|\langle n, k_{\vec{n}} | n, k_{\vec{n}+\vec{u}_i} \rangle|}, \tag{7.22}$$

where $i = x, y$, $\vec{u}_i$ is unit vector in the i direction and we write $k_{\vec{n}}$ to denote the momentum $\vec{k}$ corresponding to the grid point $\vec{n}$. The field strength, or the Berry curvature, corresponding to these link variables is then expressed as

$$\mathcal{F}_{xy}(\vec{n}) = \frac{1}{2\pi} \mathrm{Im} \ln \mathcal{A}_x(\vec{n}) \mathcal{A}_y(\vec{n} + \vec{u}_x) \mathcal{A}_x^{-1}(\vec{n} + \vec{u}_y) \mathcal{A}_y^{-1}(\vec{n}). \tag{7.23}$$

One may for instance obtain the Chern number by performing a sum on $\vec{n}$, i.e. $C = \sum_{\vec{n}} \mathcal{F}_{xy}(\vec{n})$, resembling the integral formula in the continuum. The Berry curvature this obtained is presented in Fig. 7.4. The most prominent observation we can make is that while there are fluctuations and the Berry curvature is not constant, these fluctuations do not show any singular or sharp features. To qualify this statement further we compare the Berry curvature of the triangular lattice CI to the Berry curvature of a simple two-orbital square lattice CI model. The latter is captured by a

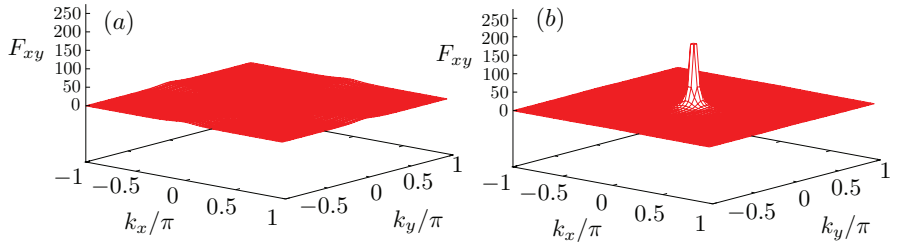

Figure 7.5: Plot of the Berry curvature for the model in (7.24) for different masses m: (a) $m = 0.8$, (b) $m = 1.9$

Hamiltonian

$$\mathcal{H}(\vec{k}) = \sin k_x \tau^1 + \sin k_y \tau^2 + (\cos k_x + \cos k_y - m)\tau^3. \tag{7.24}$$

Without discussing the physical content of this model in too much detail, we stress that the parameter m, a *mass* parameter, controls a transition from a topologically trivial regime to a topological regime with Chern number $-\text{sign}(m)$. In particular, at $m = 2$ the system is gapless and described by a low-energy Dirac theory. Close to $m = 2$ m has the interpretation f a Dirac mass. For $|m| > 2$ the insulator is trivial, i.e. $C = 0$, while for $|m| < 2$ the insulator has Chern number $-\text{sign}(m)$. In Fig. 7.5(a) and 7.5(b) we have plotted the Berry curvature for two different values of m, namely $m = 0.8$ [7.5(a)] and $m = 1.9$ [7.5(b)]. The crucial observation to be made here is the emergence of a singularity in the Berry curvature at the Dirac point as the Dirac mass approaches zero (gapless state). Such behaviour would be expected close to a topological phase transition and it is precisely such type of singular or sharp behaviour that one wishes to avoid in a CI if it is to be a good candidate for FCI physics. Indeed, at $m = 0.8$, far away from the Dirac regime the situation is similar to our triangular lattice CI model, where deviations from constant curvature are present yet smooth. In fact, all CI models that have come into view as good candidates for FCI states on various lattices, have been shown to have Berry curvatures similar to one shown in Fig. 7.4 [87,113,140]. One quantitative measure of the Berry curvature fluctuations is to calculate the standard deviation of the Berry curvature, $\overline{\sigma}_{\mathcal{F}_{xy}}$. We find for the triangular lattice CI model $\overline{\sigma}_{\mathcal{F}_{xy}} = 0.061$, which is very similar to values reported for the by now highly popular kagome CI model, see for instance [149].

To conclude this section, we come to the energetics of the triangular lattice CI. We return to the model expressed in equation (7.19) and we use the effective NN hopping t as unit of energy; the band flatness can then be tuned by varying the ratio t'/t.

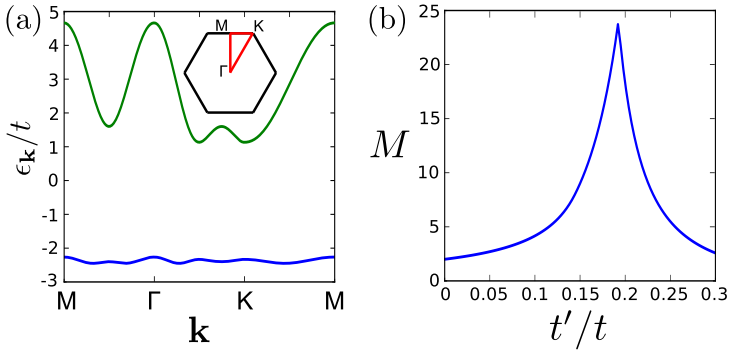

Figure 7.6: (a) Energy dispersion $E(\vec{k})$ for $t'/t = 0.2$. The inset shows the path taken through the first Brillouin zone. (b) Flatness ratio M, see Eq. (7.14), as a function of t'/t. The flatness ratio has been calculated from the dispersion along the high-symmetry directions shown in the inset on the left.

The longer range hopping t' determines the flatness of the bands of H_{kin}, which can be expressed by the figure of merit M, see Eq. (7.14). Figure 7.6 shows M depending on t', and one sees that ratios $M \gtrsim 20$ can be reached for $t' \approx 0.2$. Such flatness ratios can reasonably be achieved in the low-energy bands of a strongly correlated t_{2g} system on a triangular lattice [107]. Changing the sign of t' simply mirrors the dispersion vertically, i.e. it is then the upper band that becomes nearly flat. When going away from maximal M, the bands for smaller and larger t' differ qualitatively: For $t' < 0.2$, the Fermi surface (FS) at some fillings is almost perfectly nested.

7.4 Discussion and outlook

In the previous section we have developed and analyzed the triangular lattice Chern Insulator model from a non-interacting perspective. We have addressed the question to what extent this particular model fulfills the criteria for making a connection to the continuum Landau level problem. In order to address the question whether ground states of the CI model with interactions included actually resemble Fractional Quantum Hall states one has to resort to numerical methods. The most prominent of such numerical approaches is exact diagonalization (ED) of the Hamiltonian on a finite size cluster. Another procedure in principle appropriate to study interacting CI models is density-matrix renormalization group (DMRG) analysis, which to date has not been

used extensively, however. In the introductory section we already mentioned that to obtain FCI states the CI model is supplmented with density-density interactions, which for the present triangular lattice CI may be taken simply as (see [107, 141])

$$H_{\text{int}} = V \sum_{\langle i,j \rangle} \hat{n}_i \hat{n}_j \ . \tag{7.25}$$

There are two basic implementations of ED which have been used to study FCI states in lattice CI models. The most commen implementation uses single-particle states labeled by momentum quantum number as basis states, whereas the other approach uses real space orbitals as basis states (see [149, 150] and references therein). When using single-particle momentum eigenstates the kinetic part of the Hamiltonian is already diagonal and one needs to construct the interacting part in this basis in order to diagonalize the Hamiltonian. As such it is analogous to ED studies of the continuum problem, in which the single-particle Hilbert space consists of Landau orbitals labeled by angular momentum, and the Coulomb interaction is expanded in this basis. Another approach is to use the real space orbitals corresponding to the operators $\hat{\psi}_i$. In that case the interactions as given by equation (9.44) [or equation (7.3)] are diagonal and one needs to construct the kinetic part of the Hamiltonian in this basis. The latter approach has been used in ED studies of the triangular lattice CI [107, 141]. A widely used simplification when working in single-particle momentum space is to project out all but the flat band and in addition neglect the dispersion of this band. Working in real space effectively forces to keep the full band structure of the non-interacting CI and therefore allows to probe the interplay of energy scales.

In order to identify FCI states, i.e. states that are lattice analogs of the Fractional Quantum Hall states, one looks for spectral features that are characteristic for the Fractional Quantum Hall universality class. For instance, when the flat band is filled with a filling fraction $\nu = 1/q$, the ground state should be q-fold degenerate on the torus. On the lattice this is necessarily a quasi-degeneracy, the splitting of the ground state manifold should nevertheless vanish exponentially in the thermodynamic limit. In addition, in this limit the gap to the excited state should remain finite. Another probe of the FQH universality class is the response of the spectrum to a twist in the boundary conditions. As this represents flux threading through the handles of the torus, the ground state manifold should not be mixed with excited states upon changing the twist angle. Quasi-degenerate ground states switch places as function of inserted flux and are mapped back to themselves only after insertion of q elementary flux quanta. As a specific example of these two probes of FCI states we present results for the triangular lattice CI in Fig. 7.7 [107, 141]. The left panel, Fig. 7.7(a) shows the energy spectrum as function of total momentum, which remains a good quantum number in the presence of interactions. Three ground quasi-degenerate ground states

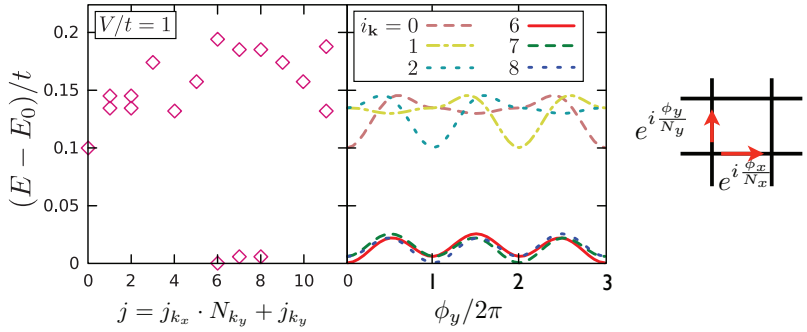

Figure 7.7: FCI state induced by NN Coulomb repulsion V in the triangular lattice CI model Eq. (7.19). (a) Energy depending on total momentum $\vec{k}$ for $V/t = 1.0$. (b) Energy depending on a flux ϕ_y added whenever an electron goes once around the whole lattice in y direction. Each addition of $\phi = 2\pi$ leads to an equivalent state, 6π to the same state. Lattice size is 4×6 sites (12 two-site unit cells), parameters in Eq. (7.19) are $t'/t = 0.2$. The filling of the flat band is $\nu = 1/3$. On the right a pictorial representation of flux insertion by adding a phase $e^{i\phi_y/N_y}$ or $e^{i\phi_x/N_x}$ to the hopping.

are clearly separated from the rest of the spectrum by an energy gap, as expected for a filling of $\nu = 1/3$. The right panel Fig. 7.7(b) shows the evolution of the ground state energies as function of adiabatic flux insertion. The spectral flow, i.e. ground states evolving into equivalent states after a single elementary flux quantum, only returning to the same state after $q = 3$ flux quanta, is in agreement with the behaviour of FQH states.

Yet another very powerful way to identify lattice analogs of FQH states is to count zero modes (ground and quasi-hole states) per momentum sector [105, 143]. For FQH states the number of zero modes per momentum sector can be obtained without diagonalizing the Hamtiltonian by just using the generalized Pauli principle applicable to the particular type of FQH state, e.g. Laughlin, composite fermion (CF), Moore-Read, ect. If the ground and quasi-hole states found by diagonalizing the FCI Hamiltonian are to be lattice analogs of the FQH states, they should obey these counting rules, as they follow from universal principles. To illustrate how such counting works for ground states we take the simplest case of a Laughlin state at filling $\nu = 1/3$, system size $N_x \times N_y = 4 \times 3$ and number of electrons $N_e = 4$. There are 12 total momenta and we organize them in a linear array with increasing j_x, i.e.

$[(j_x = 0, j_y = 0), (0,1), (0,2), (1,0), (1,1), (1,2), (2,0), \ldots]$. The counting rule or generalized Pauli principle applicable to this case dictates that no more than one electron can occupy three consecutive orbitals, respecting periodic boundary conditions in j. There are three different ways of distributing 4 electrons over 12 orbitals respecting these rules. Summing the total momenta we obtain the three total momenta $(j_x, j_y) = (2,0), (2,1), (2,2)$. Comparing this to the specific case of the triangular lattice CI, such as presented in Fig. 7.7, which has the appropriate system size and number of electrons, using that $j = j_x \cdot N_y + j_y$, we observe that the counting agrees with numerical data.

We conclude this chapter by mentioning two features of Chern Insulator and Fractional Chern Insulator models that clearly set them apart from the continuum Landau level problem in an external magnetic field. In Chapter 1 it was demonstrated that each filled Landau level contributes e^2/h to the Hall conductivity and a Landau level therefore has Chern number one. Chern insulators mimic this in the sense that an electronic band has nonzero Chern number. While the Chern number of an electronic band in most CIs is indeed one, it is possible to construct a model in which Chern bands have higher Chern number. These bands are topologically distinct from Landau levels, as they differ in topological index. This allows for the possibility to study Fractional Quantum Hall physics starting from a Chern band with higher Chern number, a possibility which does not exist for magnetic field induced Landau levels.

A second intriguing generalization of ordinary Fractional Quantum Hall physics is to consider Quantum Spin Hall insulators instead of Chern Insulators. For the present purpose, a Quantum Spin Hall insulator may be thought of as two copies of a Chern insulator, with opposite Chern character the spin-up and spin-down states (assuming there is an invariant spin-rotation axis). Combining CIs in such a way restores time-reversal invariance and adding interactions to a fractionally filled band may lead to a time-reversal invariant analog of incompressible fractional quantum Hall liquids.

These two examples of possible generalizations point to exciting potential of FCIs to uncover new physics and lead to the discovery of new states of matter.